DESIGN AND OPTIMIZATION OF A CENTRIFUGAL PUMP AS PART OF MECHANICALLY PUMPED FLUID LOOP COOLING SYSTEM FOR SPACECRAFT

Oana DUMITRESCU[1], Ionuț – Florian POPA[2]

The current paper describes the approach for the design and numerical analysis of a centrifugal pump to be part of a Mechanically Pumped Fluid Loop System which shall equip a satellite or spacecraft. Considering that the pump should work up to 15 years in space in steady conditions (large thermal gradients, with no pulsations), a centrifugal rotor along with two types of spiral casings are investigated from numerical point, having as input the nominal duty point (flow rate and pressure rise) and the type of working fluid for the Mechanically Pumped Fluid Loop (MPFL) system which targets the Orion MPCV (Multi-Purpose Crew Vehicle) module.

Keywords: centrifugal pump, impeller, spiral casing, CFD analysis, Mechanically Pumped Fluid Loop, spacecraft

1. Introduction

The nowadays spacecraft and satellites require more and more electrical power as the complexity of the payloads increases, thus generating large quantities of residual heat. If not properly evacuated, this heat can affect the on-board systems of the spacecraft, leading to malfunctions. In this regard, a thermal control system shall be featured on the spacecraft. Passive thermal control systems, such as multi-layer insulation or radiators are extensively used in this domain; however, they cannot evacuate large amounts of heat. For this purpose, active thermal control systems (ATCS) in the form of Mechanically Pumped Fluid Loops are of great interest for this domain, with important advantages over the passive systems [1]. They consist of a closed circuit in which a liquid with good heat transport properties is circulated under the action of a pump.

Such systems for spacecraft thermal control are not new, dating since the Gemini program implemented by NASA [2], when a positive displacement pump

[1] PhD student, Doctoral School of Power Engineering, University POLITEHNICA of Bucharest, CSIII at Romanian R&D Institute for Gas Turbines COMOTI, Romania, e-mail: oana.dumitrescu@comoti.ro;

[2] PhD student, Doctoral School of Aerospace Engineering, University POLITEHNICA of Bucharest, CSIII at Romanian R&D Institute for Gas Turbines COMOTI, Romania, e-mail: ionut.popa@comoti.ro;

was used. In the late 1970s ESA (European Space Agency) also started studying and developing space-qualified MPFL systems for spacecraft [3]. Although there are many pump architectures which can be successfully applied for this application, one of them stands out in the literature, namely the canned pump type, with the electric motor integrated in the housing. This allows using more compact pumps, but the assembly becomes more complex, as it requires dedicated internal circuits for cooling and lubrication. Such a canned-type pump was designed and developed for the Columbus module as part of the International Space Station, ensuring a flow rate between 100 and 850 kg/h and a pressure rise up to 4 bar, with water as working fluid [4].

Currently there are several pumps in development for MPFL systems, both centrifugal and positive displacement type. At European level the ones that can be remarked are the pumps produced by Realtechnologie AG, currently Nanospace AG Switzerland – Fig.1. A synthesis on the on-going pump developments for space applications is presented in [5].

Fig. 1. Family of pumps for MPFL systems developed by Realtechnologie AG (now Nanospace) [5]

The centrifugal pump discussed in this paper targets the Orion MPCV (Multi-Purpose Crew Vehicle), a space module partially reusable, developed by NASA for space programs involving manned space missions [6]. The nominal duty point for this application is 750 kg/h and 2.1 bar pressure rise using HFE-7200, a working fluid with good heat transport properties developed by 3M. In the following paragraphs the authors present the theoretical approach for the design of such a pump, followed by a numerical analysis of the hydraulic part (impeller and spiral casing) of the pump.

2. Geometry definition

Centrifugal pump design can be established based on various criteria, such as: fields of pump application, process and design requirements pump medium,

operational cost etc. A centrifugal pump can operate at different flow rates and corresponding pumping heads, modifying power and efficiency. The quantity of liquid that passes through the pump and the energy exchange that takes place can be quantified by functional parameters, like mass flow, head, power, efficiency and rotational speed. Among the factors that contribute on pump selection process are lifecycle cost analysis, commercial availability, main process parameters (flow, pressure, temperature etc.), fluid type, working parameters capacity, head, suction and discharge pressures etc.

The pump efficiency is influenced by energy losses as hydraulic losses due to fluid friction and turbulence, volumetric losses caused by leaks through internal gaps, mechanical losses due to friction in bearings, with housing etc. Using performance parameters, hydraulic power and total efficiency are expressed as:

$$P_{hydraulic} = \omega \cdot T = \omega \cdot (U_2 C_{u2} - U_1 C_{u1}) = Q \cdot \gamma \cdot H_{pump} \quad (1)$$

$$\eta = \frac{Q \cdot \gamma \cdot H_{pump}}{P_{shaft}} = \eta_m \cdot \eta_v \cdot \eta_h \quad (2)$$

with P_{shaft}– shaft power, η_m – mechanical efficiency, η_v - volumetric efficiency, η_h - hydraulic efficiency, γ - specific weight.

The hydraulic part of the pump consists of two components, the impeller (usually centrifugal) and a spiral casing. Together they ensure the flow of the working fluid in the MPFL system by converting the kinetic energy of the fluid entering in the impeller into pressure energy [1].

The *impeller shape* was designed to satisfy the input parameters and to ensure high performances, specific to the pump type and operating range. Using triangle theory, the blade inlet and exit angle are determined and described in Fig. 2, where are represented the velocity vectors for inlet and outlet. The parameters considered in the figure represent: *C* as absolute velocity of the fluid, *W* the relative velocity, *U* the impellers tangential velocity, α the angle between the absolute velocity and the tangential component and β the angle between the relative velocity and tangential velocity. Further, impeller components denoted with *1* represent inlet conditions and with *2* outlet conditions. The angles β_1 and β_2 determine the direction of the relative velocities *W* and are called constructive angles of the rotor.

The blade inlet angle is determined based on the velocity triangle theory, and considering the minimum shock condition at the entrance can be written as:

$$tg\beta_1 = \frac{C_{m1}}{U_1}, \text{ where } C_{m1} = \frac{Q}{A_1} \quad (3)$$

where C_m component of absolute velocity in the meridional plane, A_1 inlet area, *Q* volumetric mass.

From the continuity equation, at impeller inlet, is defined the volumetric flow rate:

$$Q_c = \pi D_1 b_1 C_{m1} \text{ , } b_1 = \frac{Q_c}{\pi D_1 C_{m1}} \tag{4}$$

with b_1 the blade height.
The same relation (4) also applies for the blade outlet height. Another important aspect in defining the impeller geometry is β_2 angle, which in practice is recommended to be less than 30º [8], and its value can be determined using:

$$tg\ \beta_2 = \frac{C_{m2}}{U_2 - C_{u2}} \tag{5}$$

with C_{u2} peripheral component of absolute velocity in the outlet area.

The impeller calculated for the current paper is a centrifugal one, having six backward curved blades and 30 mm in diameter, with the impeller eye diameter of only 11 mm.

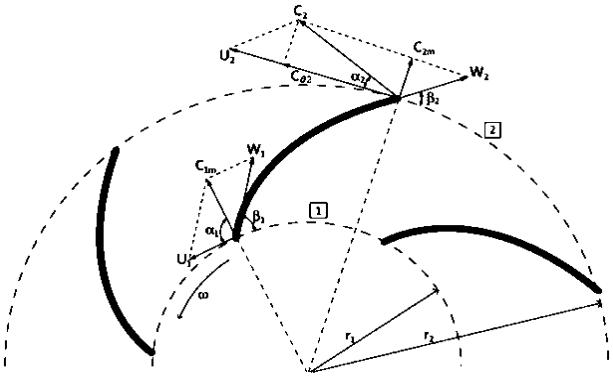

Fig. 2. Velocity diagram for a centrifugal pump [7]

For the *spiral casing*, two designs were investigated (designated ***A*** and ***B***), with different cross section inlet types. Considering the values obtained for the spiral casing cross section diameters, the first cross sections are elliptical, with areas equivalent for the diameter obtained by calculus. Elliptical cross-section areas have a small advantage over the rest of types, due to smaller friction losses [9] and higher-pressure head [10]. Also, a volute with a larger flow area can assure a wider higher – efficiency region [11]. After the final spiral casing cross section, the outlet is conical, with an angle between 8° to 12°, limited to the MPFL piping diameter, established at 16 mm.

Both spiral casings are design using a constant circumferential velocity approach, applying the following equation:

$$c_u \cdot r = const. \tag{6}$$

Another important parameter in pump design is the radial gap ($\Delta r = (D_3 - D_2)/2$), D_3 – diameter to volute basic circle) between impeller and spiral casing tongue. If the gap is too small, pump efficiency increases, but could cause

cavitation near spiral casing tongue; otherwise, if radial gap increases, pump efficiency will decrease, then again will improve pump vibration and cavitation [12].

3. Numeric simulation analysis

CFD (Computational Fluid Dynamics) analysis is one of the most important aspects in defining the geometry of a pump. Such type of analysis can provide details about the performance of the pump before manufacturing and testing, being able to ensure performance prediction at different operating conditions, like: cavitation analysis, parametric study, analysis of component interaction etc.

In the present study, the problem is defined as a steady state case for an incompressible fluid, HFE 7200 ($\rho = 1430\ kg/m^3$), with physical properties and material description defined in [13].One important characteristic of HFE 7200 over water, which is a widely used fluid in pump simulations, is given by density value, being with 40% much higher.

Material properties are defined for a reference temperature of 25ºC.

a) Mesh independence

Before solving the flow motion, grid size is studied, in order to offer a proper description of the flow. In their research, Drăgan et al. [14] found that mesh convergence depends significantly on the operating point, while grid size is invariant with mass flow assessment. Also, grid size and width proximity have significant impact on flow characteristics as: large width and fine grid conduct to longer computational time, while a coarse grid and small width offers a poor description of flow features [15].

To determine the convergence of the numerical solution, a grid sensitivity study was performed on the pump impeller. The process consists of five grid resolutions, starting with a coarse mesh and ending with the fine one; all numerical simulations respect the same operating conditions and fluid properties. For all grids was kept the first cell size, having a value of y+ as closed to one as possible. Around the blade region, the grid was refined, in order to capture any physical phenomena that could occur in the turbulent boundary layer.

The computational grid was created using Numeca/Fine Turbo program, and the numerical simulations were performed with Ansys CFX solver, applied for the incompressible Reynolds averaged Navier-Stokes model. Impeller mesh was generated using a blocking scheme, with hexahedral elements, offering better convergence and higher resolution over unstructured grids [16].

To assess the grid independence study, pump head was chosen as comparative parameter. Convergence criteria represent another factor that is used

as quality and evaluation control in CFD analysis. For a good convergence, the residual values were monitored all the time until reaching a steady solution and the tolerance of the residual was set to 10^{-5} for continuity and velocity components. Also, overall imbalance for the domain variables was less than 1%.

Figure 3 presents the grid independence study of different mesh distributions. Depending on the geometry complexity, the grid size can lead to high computational costs or to poor results caused by discretization or truncation errors. In order to decrease the computation time, offering a much faster solution, the numerical analysis that studies grid influence was performed only for one impeller channel with periodic interfaces to adjacent blades.

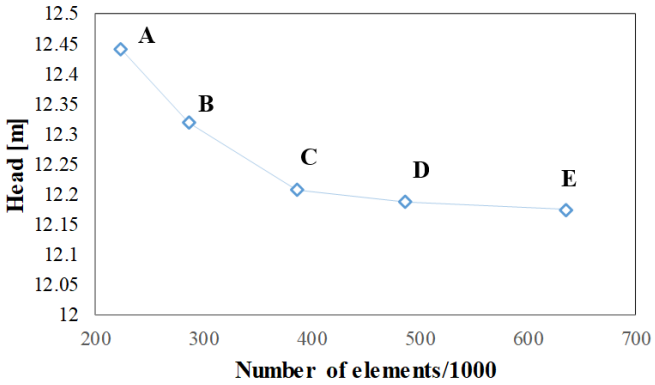

Fig. 3. Head variation for the grid independence study

Pursuant to Fig. 3, as the mesh number increases the calculated head value decreases, proving that the increase of mesh elements and quality offers more accurate results. For the present study, grid ***D*** provides a reliable description of the flow being capable of ensuring mesh independence, also offering a good compromise between coarse and fine grid.

Computational grid for the medium case has approximately 531,000 elements /channel. Figure 4 presents the impeller grid, with the proper refinement near walls and also the leading and trailing edge grid.

In order to quantify the results of the two cases, $y+$ distribution is analysed. Figure 5 illustrates $y+$ dispersal for the radial impeller. A maximum value of 3.5 is obtained at the impeller trailing edge, but the overall impeller value is below 4, representing a low value that highlights the quality of the grid and satisfies the Shear Stress Transport (SST) turbulence model.

b) Turbulence model

Another key aspect in defining a CFD process is represented by the turbulence modelling. There is a strong relation between the grid size and turbulence model, as presented by Dumitrescu et al. in [17], suggesting that with a

calculation grid above 5 mil cells/passage, RANS (Reynolds Averaged Navier Stokes) models become unstable and ensure poor convergence. Mao et al. [18] compared experimental results of a centrifugal pump with numerical ones, observing that SST turbulence models offer close results in predicting head. Another paper providing good agreement between experimental measurements and numerical simulations is presented by Casimir et al. [19].

All numerical simulations presented in this paper are realized using SST as turbulence model. This model is considered to be a hybrid one, by combining k - ε and k – ω turbulence models to increase the accuracy of the flows and to capture the effects of boundary layer separation [20]. However, each model has disadvantages, as described by Menter [21].

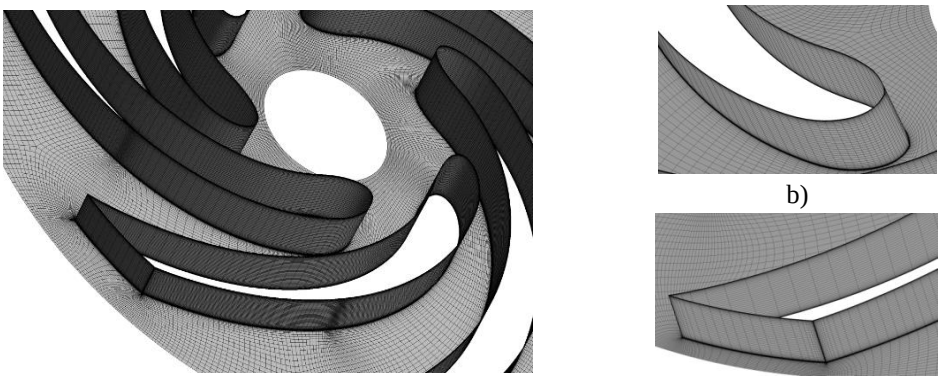

a) b) c)

Fig. 4. a) Pump impeller mesh, b) details of leading edge grid, c) details of trailing edge grid

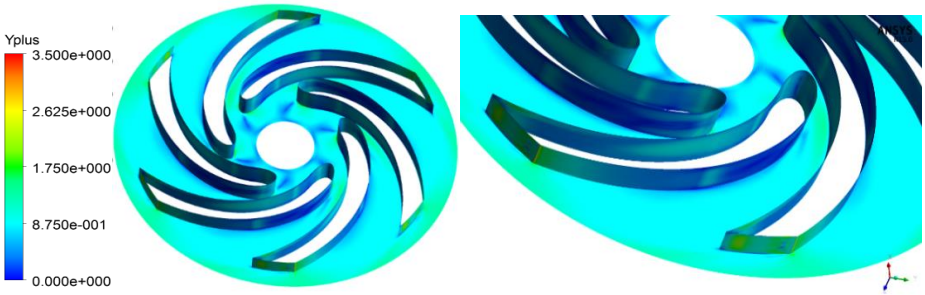

Fig. 5. Y+ distribution for the impeller

c) Boundary conditions

Numerical simulations conducted for the centrifugal pump studies the entire impeller, an important fact in the context of establishing the interaction between the rotor and the spiral casing. Impeller – spiral casing interface is influenced by the hydrodynamic interaction between the two components, with a week coupling effect, interface results for frozen rotor and circumferential

averaging, are similar but with a strong effect the results may differ for the two interface models.

This paper focuses on frozen rotor interface, which allows the determination of the azimuthal effects induced by the spiral casing. The *frozen rotor* model provides a local coupling while the impeller –spiral casing relative position is not updated at each time step, being fixed across the interface; thereby transient effects at the frame of reference are not modelled.

The boundary conditions implemented for the case are: *Inlet boundary*: total pressure of 2 bar; *Solid walls*: hub, shroud, blade, spiral casing; *Outlet boundary*: mass flow 750 kg/h.

d) Numerical simulation

For the computational part, impeller – spiral casing matching is analysed along with flow design patterns. The interaction between them is characterized by complex flows, triggering distortion in the flow structure, influencing stage performances. Further are presented the results of two numerical simulation cases that address two types of spiral casing geometries.

Total pressure distribution in meridional view is displayed in Fig. 6; illustrating those differences between the two cases are minor. Impeller of case *A)* has an area with a higher-pressure value near the spiral casing tongue, where the cross-sectional area is smaller, not allowing a uniform velocity distribution after exiting the impeller. In case *B)* the total pressure distribution is uniform in the impeller, but varies at the periphery comparative with case *A)*, which has a higher pressure in the upper-left area with respect to the lower part of the frame. Also, at the interaction between impeller and spiral casing, there are no discrepancies that could cause instabilities and affect the pump performances.

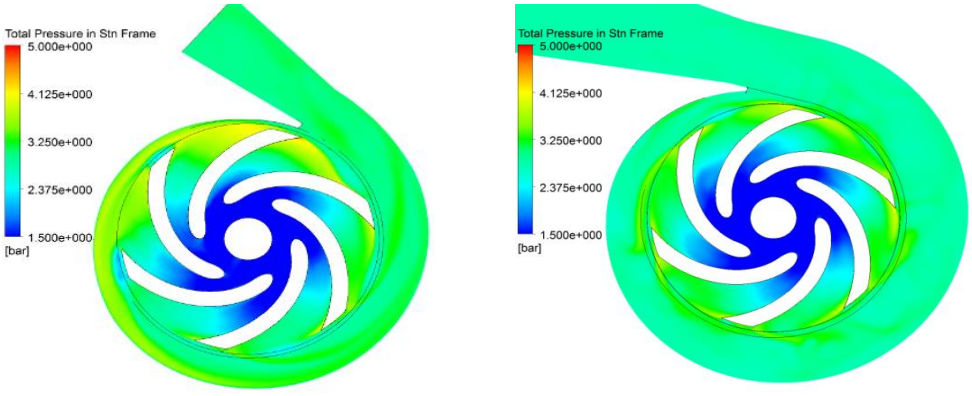

Spiral casing *A)* Spiral casing *B)*

Fig. 6. Total pressure distribution at 50% span

Figure 7 illustrates velocity distribution on the interface between impeller and spiral casing, near the spiral casing tongue. Both cases present areas with higher velocity at the interface, but case *A)* value extends through a much bigger zone, caused by a smaller cross – section area.

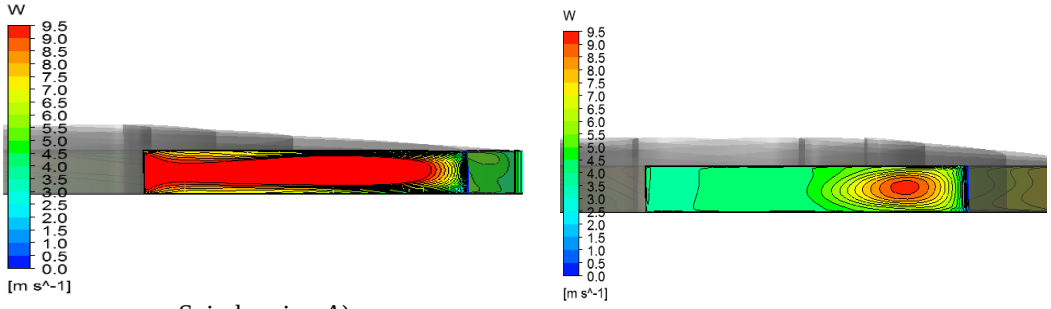

Spiral casing *A)* Spiral casing *B)*

Fig. 7. Relative velocity distribution at blade trailing edge

Figure 8 presents the locations of four spiral casing sections positioned at equal distances. Every section illustrates the velocity streamlines, where the flow structure corresponding to each area is observed. Due to increase of cross-section area of the spiral casing, the absolute velocity decreases as the fluid flow approaches the outlet zone of the pump. In spiral casing *B)* are developed two symmetrical counter rotating vortices, whose symmetry is much better defined as the area of the section increases. In the sections with a small area, the asymmetric vortices are observed, causing a lower total pressure. Total pressure losses in spiral casing *A)* are lower than in spiral casing *B)*, with a difference of approximately 0.17 bar.

Figure 9 and 10 describes the total pressure distribution and velocity in the spiral casing. Both pressure and velocity are averaged for every cross section. As the cross-section area is increasing, the velocity is decreasing from cross section *I* to spiral casing tongue, section *VIII*. For spiral casing *A)* near the tongue, the flow area is much smaller comparative with case *B)*, providing higher velocity gradient. In terms of total pressure, the value increases with the increase of the cross-section area.

Overall differences in total pressure, in the 8 planes, are small, and caused partially by the area differences of the spiral casing, especially from cross – section *I* to *III*, where casing *B)* area is higher.

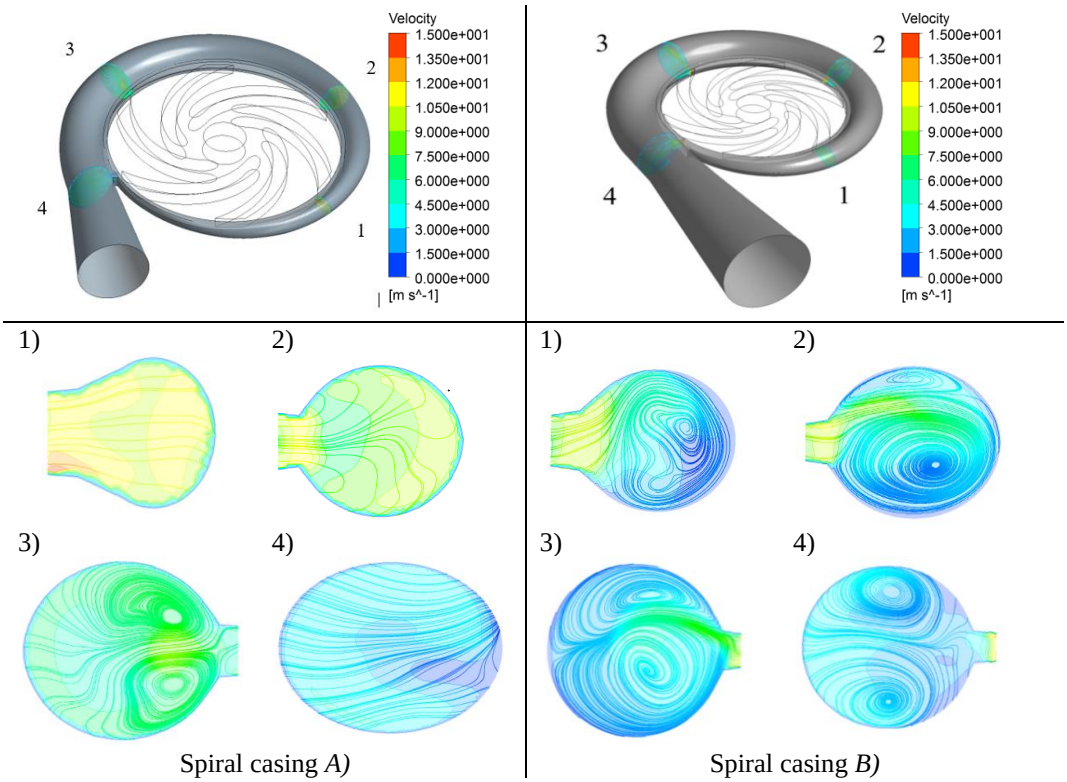

Fig. 8.Streamline contours at four different planes positioned in the spiral casing

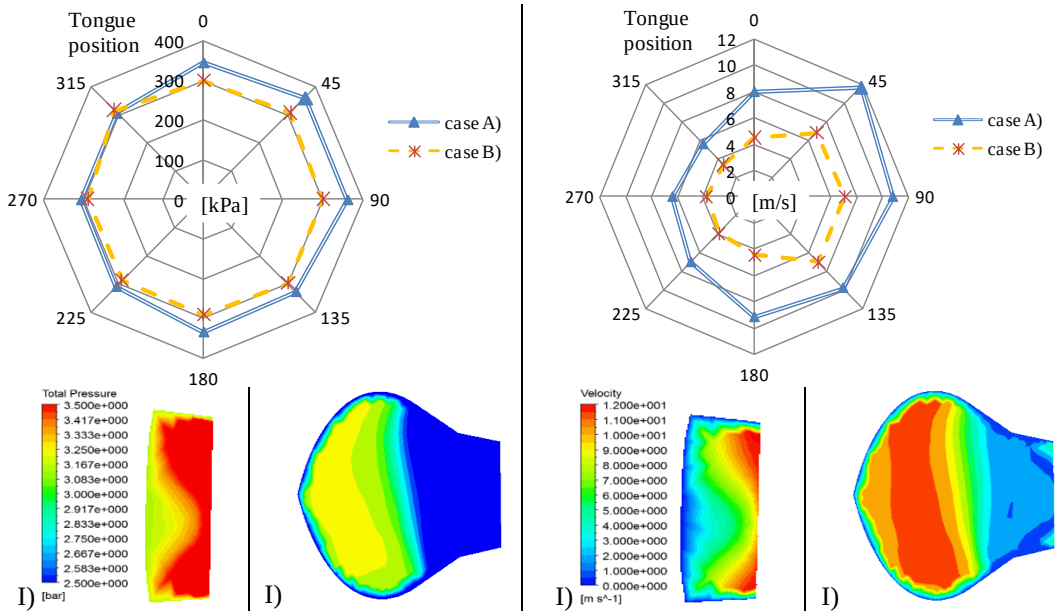

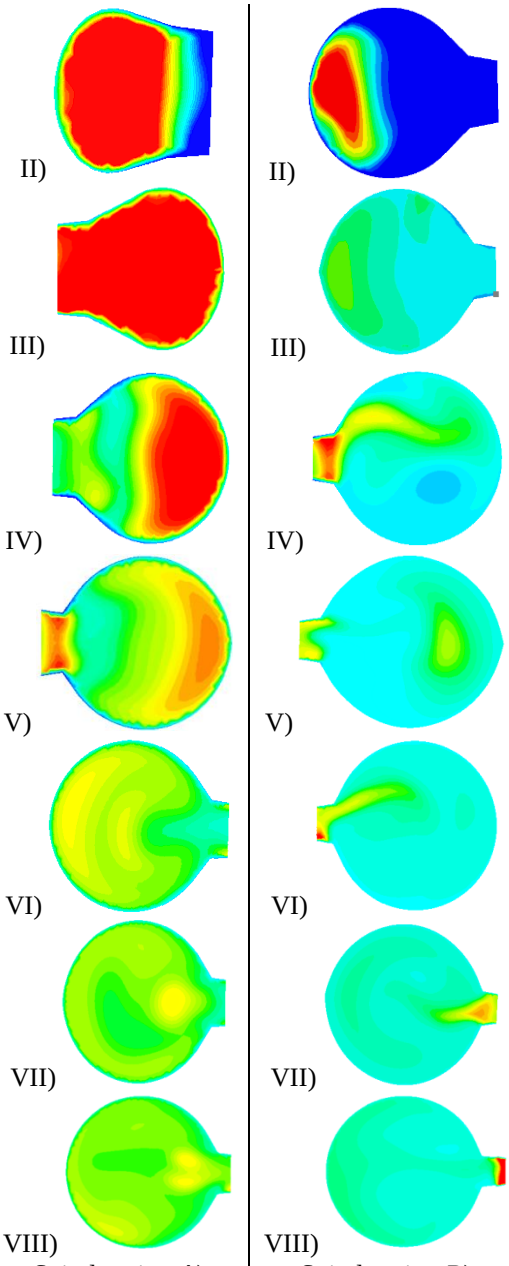

Spiral casing *A)*

Spiral casing *B)*

Fig. 9.Distribution of total pressure in spiral casing

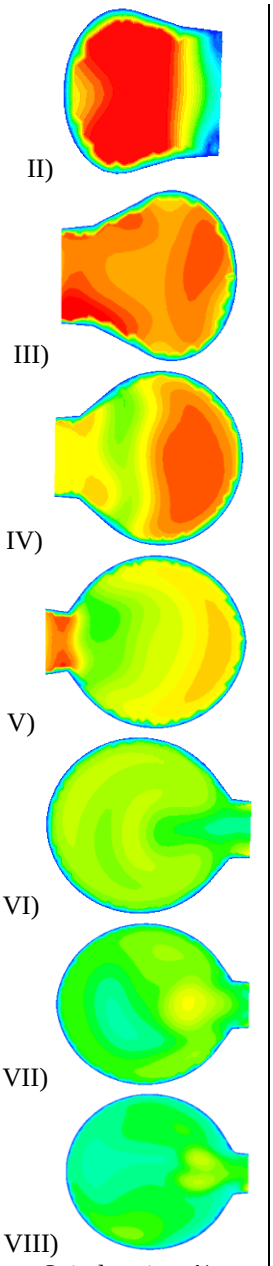

Spiral casing *A)*

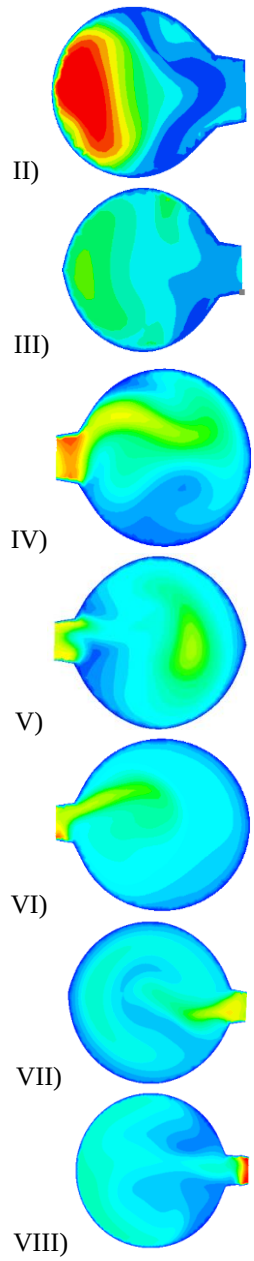

Spiral casing *B)*

Fig. 10.Distribution of velocity in spiral casing

Regardless the differences between the two cases, the local pressure is much higher than the vapour pressure that corresponds with the reference temperature (25ºC), therefore a cavitation phenomenon is not developed in this centrifugal pump.

4. Conclusions

Pump performances are influenced by the complex flow developed inside, thus flow analysis, even if it is a complex process, offers predictions about flow motion and concerning in design and off-design conditions. Computational Fluid Dynamics technique has been applied to investigate the behaviour of an incompressible fluid inside a centrifugal pump used for space applications, namely for an active thermal control system which shall equip a spacecraft. A pump was designed (impeller and 2 spiral casings) considering the nature of the working fluid and the required flow rate. Numerical simulations were performed for steady Reynolds Averaged Navier - Stokes equations with a two equations *k-ω SST* turbulence model. To offer better accuracy to the results and computational efficiency, a mesh independence study was realized for five grid sizes. Two types of spiral casing geometries were studied and compared, offering information about design importance and pump performances. The obtained results, of spiral casing *A)*, offer a pressure rise close to the one imposed by the nominal duty point, namely 2 bar. The difference being given by pressure losses in the spiral casing, especially in the area of the tongue, but improvement can also be made by increasing the impeller load. Further on, a more complex geometrical study is necessary near the cutwater point, involving also the influence of the cross-section area and unsteady analysis.

R E F E R E N C E S

[1]. *D.G. Gilmore*, Spacecraft Thermal Control Handbook, Volume I: Fundamental Technologies, Second Edition, American Institute of Aeronautics and Astronautics, The Aerospace Corporation, ISBN 1-884989-11-X, 2002;

[2]. *D. Mugurusa, M. Arner, C. Patruski, G. Adamson, H. Hansen, M. Neumann*, Development of a Low Specific Speed, Centrifugal, Mini Pump for a Two Phase Mechanically Pumped Fluid Loop,*49th International Conference on Environmental Systems*, Boston, Massachusetts, 2019;

[3]. *J. van ES, H.J. van Gerner, R.C. van Bethem, S. Lapensee, S, D. Schwaller*, Component Developments in Europe for Mechanically Pumped Fluid Loop Systems (MPLs) for Cooling Applications in Space, *46th International Conference on Environmental Systems*, Vienna, Austria, 2016;

[4]. *R. Orlando, P. Osella, M.Ferrera*, Columbus Water Pump Package Overview, *21st International Conference on Environmental Systems*, San Francisco, California, July 15-18, SAE Technical Paper Series, 1991;
[5]. IMPACTA – D2.1 – Study of the state of the art of Space Thermal Control Systems, v2, rev.0
[6]. *J.F. Lewis, R.A Barido, P. Boehm, C.D. Cross, G.E. Rains*, Orion Multi-Purpose Crew Vehicle Active Thermal Control and Environmental Control and Life Support Development Status, NASA Johnson Space Center, Houston, Texas;
[7]. *C.B. Jacobsen*, The Centrifugal Pump, Grundfos, 2010;
[8]. *N. Mohammadi, M. Fakharzadeh*, Analysis of effect of impeller geometry including blade outlet angle on the performance of multi-pressure pumps: Simulation and experiment, Mechanika 2017; vol.23, pp.107 – 119, 2017;
[9]. *R.A.Van den Braembussche*, Flow and Loss Mechanisms in Spiral casings of Centrifugal Pumps, Design and Analysis of High Speed Pumps, Educational Notes RTO – EN – AVT-143, Paper 12, pp.12-1 -12-26, 2006;
[10]. *S. Yang, F. Kong, B.Chen*, Research on Pump Spiral casing Design Method Using CFD, Hindawi Publishing Corporation, *International Journal of Rotating Machinery*, Article ID 137860, Volume 2011, 7 pages, 2011;
[11]. *Y. Tao, S. Yuan, J. Liu, F. Zhang*, Influence of Cross-Sectional Flow Area of Annular Spiral Casing on Transient Characteristics of Ceramic Centrifugal Pump, *Chinese Journal of Mechanical Engineering*, Volume 32, nr.4, 2019;
[12]. *J.Kurokawa, K. Matsumoto*, Development of high efficiency spiral casing pump of very low specific speed, *Proceedings of the 6th Asian International Conference on Fluid Machinery*, Beijing, China, pp. 250-255, 2000;
[13]. 3M™ Novec™ 7200 Engineered Fluid, Product Information, Accessed May 2021
https://multimedia.3m.com/mws/media/569860O/3mtm-thermal-management-fluids-for-military-aerospace-apps.pdf ;
[14]. *V.Drăgan, O. Dumitrescu, I. Mălael, I. Porumbel, B. Gherman, C. Puşcaşu*, Turbulence model sensitivity on steady state mapping of a very high pressure ratio compressor stage, *AIP Conference Proceedings 2046*, 020024, 2018;
[15]. *M. G. Gebreslassie, G.R. Tabor, M. R. Belmont*, CFD Simulations for Sensitivity Analysis of Different Parameters to the Wake Characteristics of Tidal Turbine, *Open Journal of Fluid Dynamics*, Vol.2, pp. 56-64, 2012;
[16]. *Z. Ali, P. G. Tucker, S. Shahpar*, Optimal Mesh Topology Generation CFD, *Computer Methods in Applied Mechanics and Engineering* 317, December 2016;
[17]. *O.Dumitrescu, V Drăgan, I Porumbel, B Gherman*, Numerical assessment of a very high pressure ratio centrifugal impeller, *IOP Conf. Series: Materials Science and Engineering* 916, 2020;
[18]. *J. Y. Mao, S. Q. Yuan, J. Pei, J. F. Zhang, W. J. Wang*, Applications of different turbulence models in simulations of a large annular spiral casing-type pump with the diffuser, IOP Conf. Ser.: Earth Environ. Sci. 22 022019, 2014;

[19].*N.Casimir, Z.Xiangyuan, G.Ludwig, R.Skoda*, Assessment as statistical eddy-viscosity turbulence models for unsteady low at part and overload operation of centrifugal pumps, *Proceedings of 13thEuropean Conference on Turbomachinery Fluid Dynamics Thermodynamics (ETC13)*, Lausanne, ETC2019-047, 2019;
[20]. Ansys Help, http://ansyshelp.ansys.com, Accessed December 2020;
[21]. *F. R. Menter*, Zonal two equation k-ω turbulence models for aerodynamic flows, *23rd Fluid Dynamics, Plasma dynamics, and Lasers Conference* AIAA-93-2906, 2012.